AFRL-RV-PS-
TR-2017-0160

AFRL-RV-PS-
TR-2017-0160

A DUAL STAGE LINEAR PREDICTION APPROACH TOWARDS WIDEBAND FM DEMODULATION WITH MULTILEVEL AND PARTIAL RESPONSE SIGNALING

Balu Santhanam and Wenjing Liu

University of New Mexico
1700 Lomas Blvd. NE
Albuquerque, NM 87106-3807

19 Jan 2018

Final Report

AIR FORCE RESEARCH LABORATORY
Space Vehicles Directorate
3550 Aberdeen Ave SE
AIR FORCE MATERIEL COMMAND
KIRTLAND AIR FORCE BASE, NM 87117-5776

NOTICE AND SIGNATURE PAGE

Using Government drawings, specifications, or other data included in this document for any purpose other than Government procurement does not in any way obligate the U.S. Government. The fact that the Government formulated or supplied the drawings, specifications, or other data does not license the holder or any other person or corporation; or convey any rights or permission to manufacture, use, or sell any patented invention that may relate to them.

This report is the result of contracted fundamental research which is exempt from public affairs security and policy review in accordance with AFI 61-201, paragraph 2.3.5.1. This report is available to the general public, including foreign nationals. Copies may be obtained from the Defense Technical Information Center (DTIC) (http://www.dtic.mil).

Qualified requestors may obtain copies of this report from the Defense Technical Information Center (DTIC) (http://www.dtic.mil).

AFRL-RV-PS-TR-2017-0160 HAS BEEN REVIEWED AND IS APPROVED FOR PUBLICATION IN ACCORDANCE WITH ASSIGNED DISTRIBUTION STATE

//SIGNED//
KHANH PHAM
Program Manager

//SIGNED//
DAVID CARDIMONA
Technical Advisor, Space Based Advanced Sensing and Protection

//SIGNED//
JOHN BEAUCHEMIN
Chief Engineer, Spacecraft Technology Division
Space Vehicles Directorate

This report is published in the interest of scientific and technical information exchange, and its publication does not constitute the Government's approval or disapproval of its ideas or findings.

Approved for public release; distribution is unlimited.

REPORT DOCUMENTATION PAGE

Form Approved
OMB No. 0704-0188

1. REPORT DATE *(DD-MM-YY)*	**2. REPORT TYPE**	**3. DATES COVERED** *(From - To)*
19-01-2018	Final Report	12 May 2016 – 27 Oct 2017

4. TITLE AND SUBTITLE
A Dual Stage Linear Prediction Approach Towards Wideband FM Demodulation With Multilevel and Partial Response Signaling

5a. CONTRACT NUMBER
FA9453-16-1-0067

5b. GRANT NUMBER

5c. PROGRAM ELEMENT NUMBER
62601F

6. AUTHOR(S)
Balu Santhanam and Wenjing Liu

5d. PROJECT NUMBER
8809

5e. TASK NUMBER
PPM00030324

5f. WORK UNIT NUMBER
EF129220

7. PERFORMING ORGANIZATION NAME(S) AND ADDRESS(ES)
University of New Mexico
1700 Lomas Blvd. NE
Albuquerque, NM 87106-3807

8. PERFORMING ORGANIZATION REPORT NUMBER

9. SPONSORING / MONITORING AGENCY NAME(S) AND ADDRESS(ES)
Air Force Research Laboratory
Space Vehicles Directorate
3550 Aberdeen Ave., SE
Kirtland AFB, NM 87117-5776

10. SPONSOR/MONITOR'S ACRONYM(S)
AFRL/RVSW

11. SPONSOR/MONITOR'S REPORT NUMBER(S)
AFRL-RV-PS-TR-2017-0160

12. DISTRIBUTION / AVAILABILITY STATEMENT
Approved for public release; distribution is unlimited.

13. SUPPLEMENTARY NOTES

14.ABSTRACT

Wideband Frequency Modulation is a popular modulation technique for satellite communications due to its ability to deal with trans-ionospheric distortion. Continuous Phase Modulation is a popular frequency modulation technique used in mobile communications due to spectral efficiency attributable to its continuous phase property and power efficiency attributable to its constant modulus property. The primary bottleneck in using continuous phase modulation is that the optimal receiver is a Maximum Likelihood receiver implemented via the Viterbi algorithm, requires precise knowledge of the memory length, requires that the modulation index be a ratio of incommensurate integers, and its complexity increases exponentially with the number of phase states. In this report, we present and analyze a generalized version of the multirate frequency transformation-electronics steered array approach developed by the authors towards wideband continuous phase modulation demodulation with memory that avoids the aforementioned problems with the Viterbi approach.

15. SUBJECT TERMS
Amplitude Modulation Frequency Modulation, Continuous Phase Modulation, Carrier to Information Bandwidth ratio, Frequency Shift Keying, Instantaneous Frequency

16. SECURITY CLASSIFICATION OF:			**17. LIMITATION OF ABSTRACT**	**18. NUMBER OF PAGES**	**19a. NAME OF RESPONSIBLE PERSON**
a. REPORT	**b. ABSTRACT**	**c. THIS PAGE**			Khanh Pham
Unclassified	Unclassified	Unclassified	Unlimited	34	**19b. TELEPHONE NUMBER** *(include area code)*

(This page intentionally left blank)

TABLE OF CONTENTS

Section **Page**

List of Figures

Figure **Page**

ACKNOWLEDGMENTS

This material is based on research sponsored by Air Force Research Laboratory under agreement number FA9453-16-1-0067. The U.S. Government is authorized to reproduce and distribute reprints for Governmental purposes notwithstanding any copyright notation thereon.

DISCLAIMER

The views and conclusions contained herein are those of the authors and should not be interpreted as necessarily representing the official policies or endorsements, either expressed or implied, of Air Force Research Laboratory or the U.S. Government.

(This page intentionally left blank)

1.0 SUMMARY

Wideband Frequency Modulations (FM) is a popular modulation technique for satellite communications due to its ability to deal with trans-ionospheric distortion [2, 3]. Contemporary methods for the demodulation of wideband FM signals either use negative feedback [5] or frequency estimation [13], or multirate frequency transformations and adaptive frequency tracking [9–11]. A particular form of digital FM, multilevel Gaussian Frequency Shift Keying (FSK) has been proposed as a solution for high bandwidth satellite communications [6]. On the wireless communication front, Continuous Phase Modulation (CPM) belongs to a class of non-linearly modulated signals with constant envelope, where the information is carried in the phase of the transmitted signal [12, 13, 14]. High spectral efficiency and suitability to nonlinear class C amplifiers used in mobile radio applications make CPM a popular modulation choice. A specific form of CPM namely Gaussian Minimum Shift Keying (GMSK) has been adopted in the Global System for Mobile communications (GSM) [13, 14]. The optimum receiver structure for CPM demodulation employs the Maximum Likelihood (ML) detector based on the Viterbi algorithm [1, 13, 14] applied to the unwrapped phase of the baseband version of the received signal. This receiver structure, however has limitations on the allowable modulation index and significant computational complexity which grows exponentially with increase in the number of phase states.

In prior work [9, 10] it was shown that frequency discrimination for full response CPM demodulation has the same performance as that of Binary Phase Shift Keying (BPSK) detection in Additive White Gaussian Noise (AWGN). In recent work [9, 11], frequency tracking based wideband FM demodulation was extended to large wideband to narrowband conversion factors using multirate frequency transformations. Frequency estimation based approaches have the added advantage that they are immune to phase distortions introduced by the channel which would adversely affect the Viterbi approach [13].

2.0 INTRODUCTION

2.1 Signal Model

2.1.1 Continuous Phase Modulation

The standard Continuous Phase Modulation (CPM) model depends on its pulse-shaping function $p(t)$, with duration length of symbol periods L and modulating symbols, i.e., binary Phase Amplitude Modulation (PAM) symbols $a[k] \in \{-1, 1\}$. The instantaneous frequency (IF) signal takes the form [13, 14]:

$$\omega_i(t) = \omega_c + 2\pi h + \sum_{k=-\infty}^{\infty} a[k]p(t - kT_b) \quad (1)$$

where ωc is the carrier frequency and h is the modulation index of CPM. The phase deviation from the carrier phase is given by:

$$\emptyset_{dev}(t; a) = 2\pi h \sum_{k=-\infty}^{\infty} a[k]q(t - kT_b) \quad (2)$$

where $q(t) = \int_0^t p(\tau)d\tau$ corresponds to the phase pulse shaping function. If *p(t)* is a rectangular pulse then this form of is referred to as L-pulsewidth CPM with Raised-cosine Pulse Shaping (L-REC) CPM, and if *p(t)* is a raised cosine pulse then this form of CPM is referred to as L-pulsewidth CPM with Rectangular Pulse Shaping (L-RAC) CPM. The CPM signal is then obtained via frequency modulation.

$$r(t) = A\cos\left(\int_{-\infty}^{t} \omega_i(\tau)\ d\tau + \theta_o\right) \tag{3}$$

Using a pulse shaping function of duration larger than a symbol period, i.e., partial response signaling introduces memory into the modulation scheme.

2.1.2 Wideband AM-FM Modulation

2.1.2.1 AM-FM Signal Model

Mono-component Amplitude-Modulation Frequency-Modulation (AM-FM) signals are time-varying sinusoids of the form:

$$s(t) = a(t)\cos(\int_{-\infty}^{t} \omega_i(\tau)\ d\tau + \theta_1) \tag{4}$$

where *Instantaneous Amplitude* (IA) is denoted by $a(t)$ and the *Instantaneous Frequency* (IF) is given by:

$$\omega_i(t) = \omega_c + \omega_m q_i(t) \tag{5}$$

Note that ω_c is the carrier (or mean) frequency and $q_i(t)$ is the normalized baseband modulated signal.

Specific for sinusoidal FM, where $a(t)$ remains a constant A, and $qi(t)$ becomes a sinusoid, the IF can be further expressed as:

$$\omega_i(t) = \omega_c + \omega_m \cos(\omega_f t + \theta_2) \tag{6}$$

Sinusoidal FM signals can be expressed via Bessel functions as:

$$s(t) = A\sum_{n=-\infty}^{\infty} J_n(\beta)\cos(\omega_c t + n\omega_m t) \tag{7}$$

where J_n is the n^{th} order cylindrical Bessel function of the first kind. The modulation index of the sinusoidal FM is defined as the ratio $\beta = \frac{\omega_m}{\omega_f}$ and the associated Carson's bandwidth is given by:

$$B = 2(\beta + 1)\omega_f \tag{8}$$

If $\beta \gg 1$, then it corresponds to the wideband FM according to the literature of FM communication systems. In addition, the *Carrier-to-information-bandwidth Ratio* (CR/IB) and the *Carrier-to-frequency Deviation Ratio* (CR/FD) are defined respectively as:

$$\frac{CR}{IB} = \frac{\omega_c}{\omega_f}, \qquad \frac{CR}{FD} = \frac{\omega_c}{\omega_m} \tag{9}$$

2.1.2.2 Mono-component AM-FM Demodulation

2.1.2.2.1 Hilbert Transform Demodulation

For a one-dimensional real-valued signal $s(t)$: R → R, we associate with it a complex-valued signal $z(t) = s(t) + j\, q(t)$, where the imaginary part $q(t)$ is defined via [2,3]:

$$q(t) = H[s(t)] = s(t) * \frac{1}{\pi t} = \int_R \frac{s(t-\xi)}{\pi \xi}\, d\xi \tag{10}$$

Note that $q(t)$ is the Hilbert transform of $s(t)$, and the complex-valued signal $z(t)$ is called the analytic signal. Assume that $s(t)$ is a real-valued AM-FM signal given as:

$$s(t) = a(t)\cos\big(\omega_c t + \phi(t)\big) \tag{11}$$

where $a(t)$ is the IA, ω_C is the carrier frequency and $\phi(t)$ is the phase for the IF $\phi'(t)$. Note that the IF defined here does not involve the carrier frequency ω_C. According to the basic property of the Hilbert transform and *Bedrosian's theorem*, $q(t)$ is the approximation to the product of the Instantaneous Amplitude (IA) and the quadrature of the FM part as:

$$q(t) = H[s(t)] \approx a(t)\sin\big(\omega_c t + \phi(t)\big) \tag{12}$$

However, this approximation is valid only if the following conditions hold:

1. $a(t)$ is a narrowband lowpass signal that varies slowly with time,

2. carrier frequency ω_c is sufficiently large such that

$$\omega_c \gg \phi'(t) \tag{13}$$

As a result, the corresponding analytic signal is of the form:

$$z(t) = s(t) + j\,q(t) \approx a(t)\exp\left[j\left(\omega_c t + \phi(t)\right)\right] \tag{14}$$

Hence, the IA $a(t)$ and the IF $\phi'(t)$ are estimated respectively by:

$$a(t) \approx \left||z(t)|\right| \tag{15}$$

$$\phi'(t) \approx \frac{\partial}{\partial t}\left(\arctan\frac{\Im\left(z(t)\right)}{\Re\left(z(t)\right)}\right) - \omega_c \tag{16}$$

2.1.2.2.2 Energy Separation Algorithm

The Energy Separation Algorithm (ESA) as summarized in [7, 8], based on the Teager-Kaiser energy operator, is widely used for mono-component AM-FM demodulation. For a continuous-time signal $x(t)$, the nonlinear Teager-Kaiser energy operator in the continuous case is given by:

$$\Psi_C[x(t)] = \dot{x}^2(t) - x(t)\,\ddot{x}(t) \tag{17}$$

where $\dot{x}(t)$ and $\ddot{x}(t)$ denote the first and second derivatives of $x(t)$ respectively. It was first introduced by Kaiser and was applied to track the energy of harmonic oscillation. For instance, the energy of the oscillatory signal $x(t) = A\cos(\omega_C t + \theta)$ can be tracked by the operator Ψ_C via

$$\Psi_c[A\cos(\omega_c t + \theta)] = (A\omega_c)^2 \tag{18}$$

The energy operator can be further used to analyze the oscillation of signals with time-varying amplitude and frequency. By applying the energy operators Ψc on the AM-FM signal, the IA $a(t)$ and IF $\omega_i(t)$ (excluding the carrier frequency ω_c) satisfy the following relation:

$$\Psi_c[a(t)\cos(w_c t + \int_0^t \omega_i(\tau) + \theta)] \approx \left[a(t)\left(\omega_c + \omega_i(t)\right)\right]^2 \tag{19}$$

As a result, the IA $a(t)$ and the IF $\omega i(t)$ of an AM-FM signal $x(t)$ can be estimated via the Continuous Energy Separation Algorithm (CESA) summarized by:

$$\frac{\Psi[x(t)]}{\sqrt{\Psi[x'(t)]}} \approx |a(t)| \tag{20}$$

$$\sqrt{\frac{\Psi[x'(t)]}{\Psi[x(t)]}} - \omega_c \approx \omega_i(t) \tag{21}$$

where we assume that the IA $a(t)$ and the IF $\omega_i(t)$ do not vary too fast or too greatly in value compared to the carrier frequency ω_c.

2.1.2.3 Carrier Frequency and Amplitude Estimation

The carrier frequency and the amplitude of the AM–FM signal can then be estimated from the IF and IA estimates from either algorithm by simple averaging or weighted averaging:

$$\widehat{\omega}_c = \frac{1}{T}\int_0^T \widehat{\omega}_i\,(t)dt$$

$$\hat{A} = \frac{1}{T}\int_0^T \hat{a}_i\,(t)dt \tag{22}$$

This is a direct consequence of the fact that both these approaches are bandpass estimation approaches whereas traditional in-phase and quadrature demodulation, employed in narrowband communication systems, is a baseband estimation approach that requires prior knowledge of the carrier frequency.

2.1.2.4 Multirate Frequency Transformations

In the author's recent work, frequency transformations enacted via multirate signal processing were used for wideband FM to narrowband FM conversion to enable a wider range of wideband FM signals [9, 11]. The goal of the multirate processing module is to compress the bandwidth of the FM signal, however, this is accompanied by a corresponding reduction in the carrier frequency of the FM signal. To compensate for this, a heterodyning module that translates the FM signal in frequency is introduced. After the multirate heterodyne combination, the FM signal has CR/IB and CR/FD parameters in a range where standard narrowband mono-component FM demodulation algorithms work optimally. Specifically, the ESA works very well in combination with the MFT approach and will be employed in this report [11].

The IF estimates of the demodulation algorithm are then post-smoothed via simple binomial smoothing to remove high frequency fluctuations from the IF. The smoothed IF estimates are then frequency shifted and decimated to yield IF estimates of the wideband FM signal. In recent work, by rearranging the order of the systems, and via appropriate use of the Noble identities, it was shown that large wideband to narrowband conversion ratios as large as $R = 128$ can be realized [11].

The Multirate Frequency Transformations (MFT) framework specifically allows for demodulation of a CPM signal with a large modulation depth. Since the approach is based on IF estimation the approach does not encounter the rational modulation depth problem seen in the Viterbi algorithm. The basic MFT framework is shown in Figure 1.

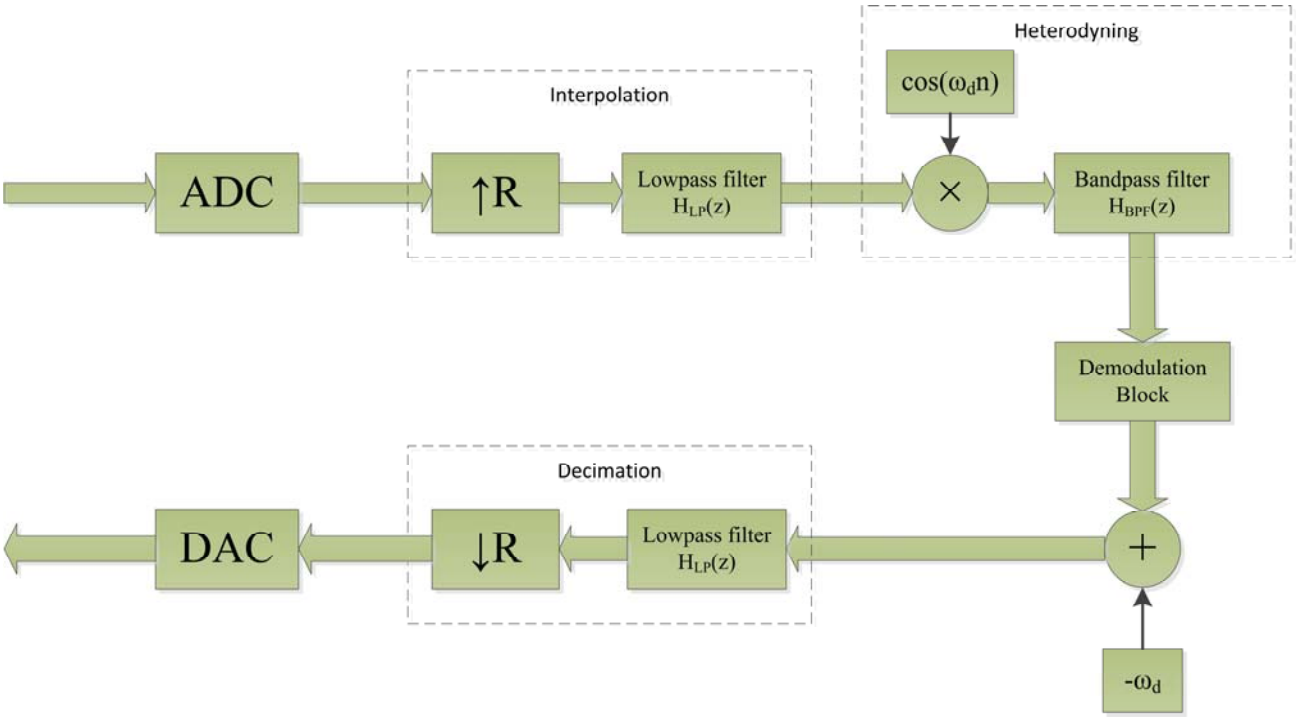

Figure 1. Block Diagram of the Basic MFT Framework

The wideband signal is first sampled above the Nyquist rate, interpolated by a factor R and then heterodyned by multiplication with $\cos(\omega_d n)$, followed by a discrete Finite Impulse Response FIR bandpass filter with a passband gain to achieve the MFT. Then it goes through a demodulation block to generate IF estimates of the compressed heterodyned signal. To obtain the IF of the original signal, the compressed heterodyned IF is then shifted back by subtracting ω_d, decimated by R and scaled back appropriately, followed by the Digital to Analog Convertor DAC module.

2.2 CPM Demodulation and the Viterbi Algorithm

As specified earlier, the standard approach for CPM demodulation is to first apply an in phase-quadrature transformation to the CPM signal to transform the passband signal to baseband, followed by the phase estimation via the Hilbert transform and phase unwrapping. The Viterbi algorithm is then applied to detect the information symbols and is a maximum likelihood sequence detection algorithm [1] that searches for the most likely path based on the received signal. However, some constraints are imposed on the modulation signal due to its finite-state machine mechanics. The modulation index must be of the form:

$$h = \frac{m}{p} \tag{23}$$

where m and p must be relatively prime positive integers, otherwise the phase trellis cannot be formed correctly since the phase states would not be distinct. As for the proposed method, unlike the phase unwrapping involved in the Viterbi, the IF can be uniquely determined, therefore such a constraint is not an issue.

Another dilemma for the Viterbi algorithm is the computation complexity that rises with the modulation complexity of the CPM signal. For a multilevel partial response CPM signal with pulse length L and symbol alphabet size M, the number of states is

$$N_s = \begin{cases} pM^{L-1} & (even\ m) \\ 2pM^{L-1}, & (odd\ m) \end{cases} \tag{24}$$

As for the proposed method, the computation complexity is not dominated by the modulation complexity of the signal. It depends primarily on the pre-determined conversion factors used for the multirate frequency transformations.

In this report, we apply the joint Multirate Frequency Transformation-Electronics Steered Array (MFT-ESA) approach to wideband CPM demodulation specifically to the following challenging environments:

1. **Large h scenarios**: this corresponds to the wideband FM regime, where the MFT will provide the maximum gain [11].

2. **Large h and multilevel** CPM that corresponds to larger bandwidths described in the M-ary FSK system proposed in [6] for satellite communications.

3. **Large h, multilevel CPM with memory**, an environment that was not addressed in prior work.

Simulation results will illustrate the efficacy of the proposed approach even in these challenging situations where the Viterbi algorithm encounters difficulties.

3.0 METHODS, ASSUMPTIONS, AND PROCEDURES

3.1 Performance of the MFT-ESA Approach

3.1.1 Binary CPM Demodulation

3.1.1.1 Binary 2-REC CPM Demodulation

First, we look at a case of binary Binary CPM with Rectangular Pulse Shaping (2-REC CPM) with a large modulation index and with memory introduced, as illustrated by Figure 2. As we can observe from Figure 3(a), the IF distortion incurred by the direct Hilbert transform demodulation and the ESA demodulation approaches are significant, while the MFT and ESA combination closely tracks the IF with little distortion. To quantify the result, the Normalized Mean Square Error (NMSE) for direct Hilbert Transform Alone (HTDA) demodulation and ESA demodulation are 0.3134 and 0.1264 respectively. By combining the MFT framework with ESA, the NMSE can be reduced to 0.0063.

3.1.1.2 Carrier Frequency Estimation

The IF estimate of the MFT-ESA in the specific case of CPM takes the form of:

$$\widehat{\omega}_i(t) = \omega_c + 2\pi h \sum_{k=-\infty}^{\infty} a[k] h_f\,(t - kT_b) + \varepsilon_\omega(t) \tag{25}$$

$h_f(t)$ corresponds to the pulse shaping function and $E_W(t)$ corresponds to zero-mean IF noise, which unlike the observation noise is not white. Assuming equiprobable symbols and taking expectations on both sides yields:

$$E\{\widehat{\omega}_i(t)\} = \omega_c \tag{26}$$

In practice, since prior knowledge of distributions is not available, we replace the expectation with a simple time-average:

$$\widehat{\omega}_c = \frac{1}{T}\int_0^T \widehat{\omega}_i\,(\tau)d\tau \tag{27}$$

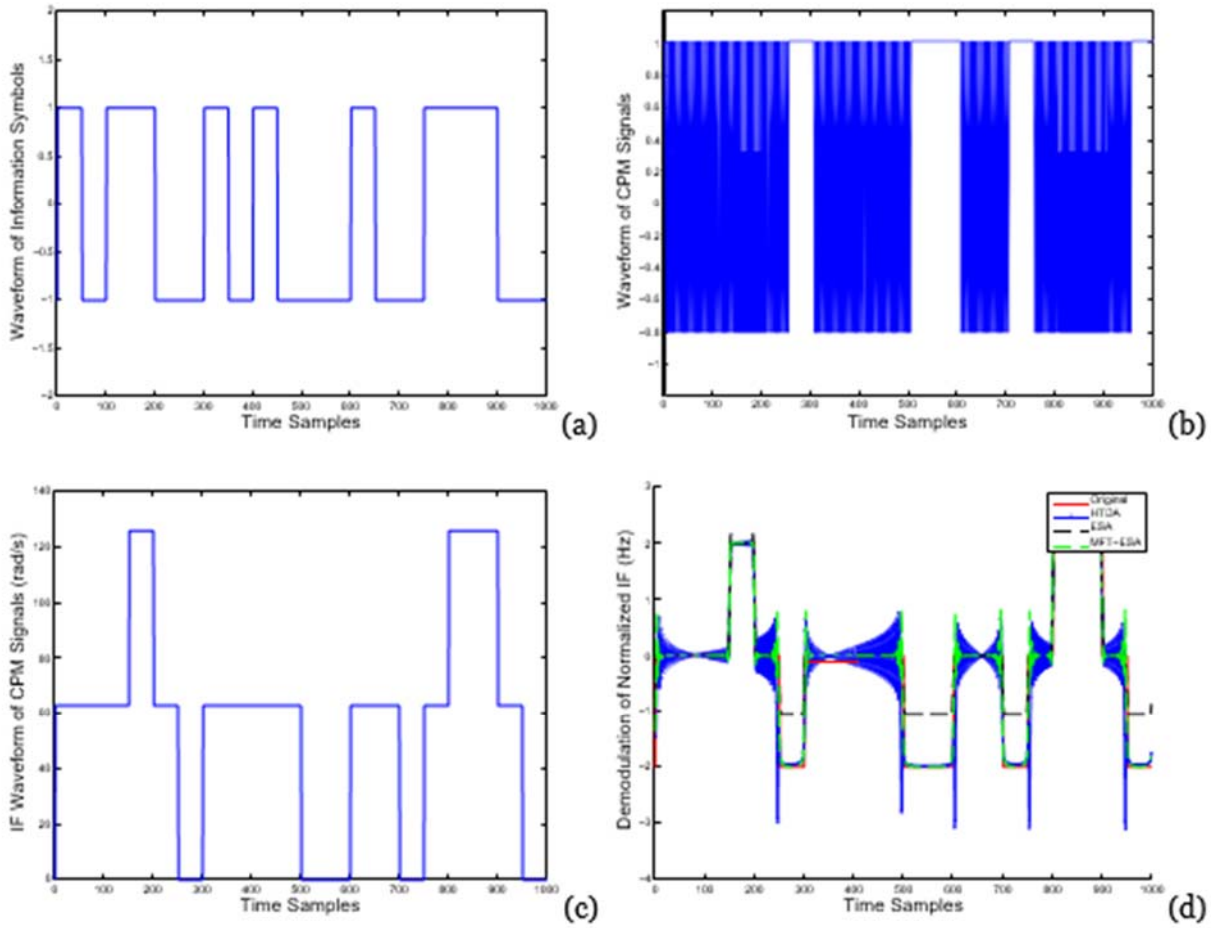

Figure 2. Binary 2-REC CPM with a Large Index

(a) Modulating symbol waveform, (b) Binary 2-REC CPM waveform, (c) IF waveform of the binary 2-REC CPM using rectangular pulse shaping function with memory introduced with parameters $h = 10$, $f_C = 10\ Hz$, and $f_S = 50Hz$ and (d) estimated IF for Hilbert transform demodulation (blue), ESA demodulation (black), and the MFT-ESA combination (green).

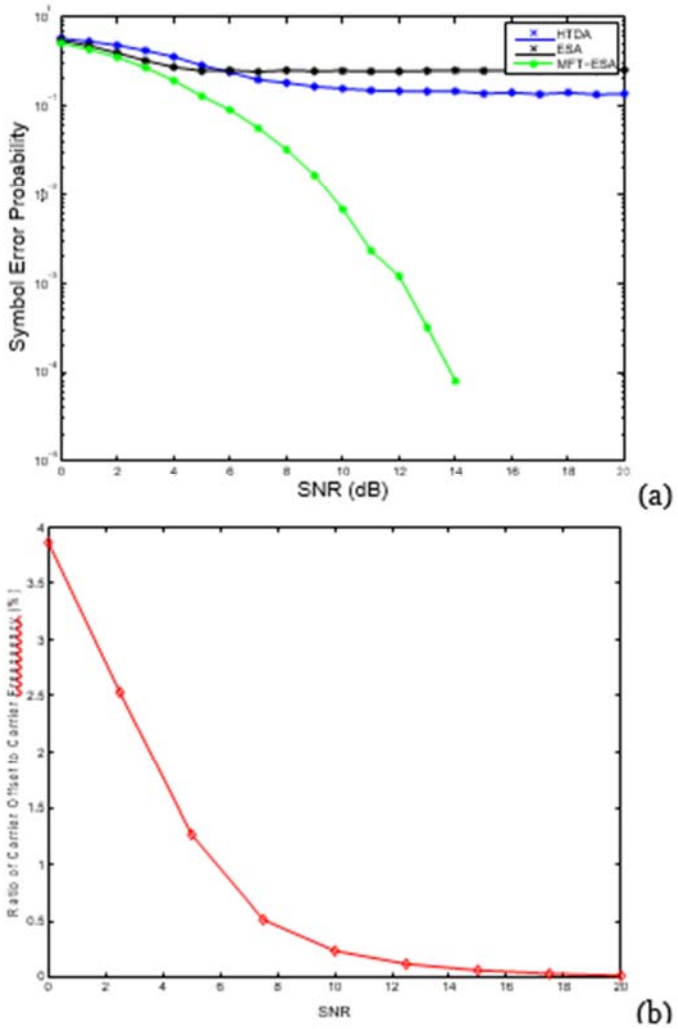

Figure 3. Performance

(a) Symbol error probability with binary 3-REC CPM for the mixed symbols after IF estimation using h = 12, f_C = 12 Hz, f_S = 50 Hz, and R = 64 and (b) carrier frequency estimation error associated with the carrier frequency estimates for the MFT-ESA approach.

In the discrete-time case, we simply replace the integral with a time-average sum:

$$\widehat{\Omega}_c = \frac{1}{L}\sum_{k=0}^{L-1}\Omega_{\mathrm{i}}[k] \tag{28}$$

Figure 3(b) depicts the carrier frequency estimation error of the MFT-ESA for the case where we have equiprobable symbols versus Signal-to-noise Ratio (SNR). For larger SNR values, the carrier-frequency estimation error goes to zero indicating that the IF yields a reliable carrier frequency estimate.

3.1.1.3 Effect of Pulse Shape: Binary 2-RAC CPM Demodulation

Another case of binary 2-RAC CPM with large modulation index and memory introduced is illustrated by Figure 4. From Figure 4, the IF distortion incurred by direct Hilbert transform demodulation and ESA demodulation are significant, while the MFT and ESA combination closely tracks the IF with little distortion. To quantify the result, the NMSE for direct HTDA demodulation and ESA demodulation are 0.0867 and 0.0654 respectively. By combining the MFT framework with ESA, the NMSE can be reduced to 0.0031. Compared with the previous 2-REC CPM with memory, we can also see that the MFT-ESA demodulation method achieves better demodulation performance for CPM with a raised cosine pulse shaping function than that obtained using a rectangular pulse shaping function. This is attributed to the inherent interpolation process in the MFT demodulation approach, which is more error-sensitive to discontinuous waveforms, such as rectangular pulses used in REC-CPM. This observation is further confirmed in Figure 4(e), where the symbol error probabilities for 1-REC-CPM, 1-RAC-CPM, and other pulse-shaping functions, are compared to illustrate the effects of the pulse shape on the performance of the MFT-ESA approach on CPM signals with parameters $f_C = 5Hz$, $f_S = 50Hz$, $h = 15/12$, $R = 16$. Formation of the phase trellis in this case would not be possible using the Viterbi algorithm since the integers m and p are commensurate. The MFT-ESA approach does not have this restriction on the modulation index since the demodulation is based on the IF of the CPM signal.

3.1.2 Multilevel CPM Demodulation

We look at a more complex case of the multilevel CPM with memory introduced, as illustrated by Figure 5. Like previous cases, from Figure 5 we can observe that the IF distortion incurred by direct Hilbert transform demodulation and ESA demodulation are also significant, while the MFT and ESA combination closely tracks the IF with little distortion. To quantify the result, the NMSE for direct HTDA demodulation and ESA demodulation in the multilevel case are 0.0624 and 0.0247 respectively. By combining the MFT framework with ESA, the NMSE can be reduced to 0.0052.

The 3-REC multilevel CPM signal with symbols taking values in $\{-3, -1, 1, 3\}$ with modulation index $h = 4$ is depicted in Figure 5. The resultant frequency deviation of the IF is equal to the carrier frequency in this extreme case. The symbol error probability associated with the mixed symbols for the MFT-ESA approach for 3-REC-CPM extracted from the IF estimates is

depicted in Figure 6. Note that 3-REC CPM signal has memory, hence the symbols determined here refer to the symbols mixed by the original modulation symbols because of memory. As the SNR increases, the MFT and ESA combination reduces the error dramatically and eventually drops to zero after a certain SNR threshold, while the error performances of the Hilbert transform (HTDA) and the ESA gradually saturate at certain levels due to carry-over effects from incomplete demodulation.

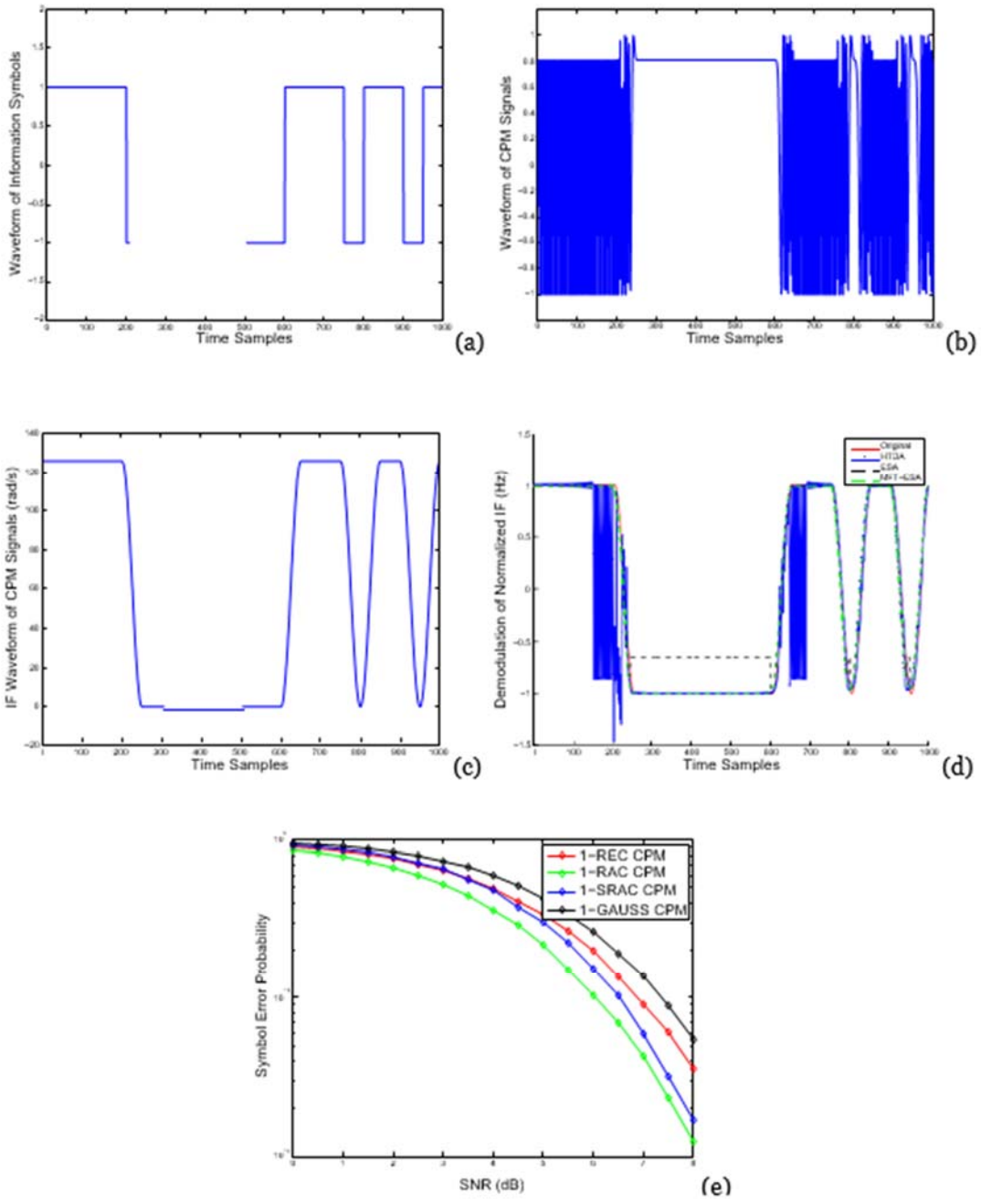

Figure 4. Binary 2-RAC CPM with a Large Modulation Index $h = 10$

a) Modulating symbol waveform. b) Binary 2-RAC CPM waveform. c) IF waveform of the binary 2-RAC CPM using raised cosine pulse shaping function with memory introduced, (d) estimated IF using Hilbert transform demodulation (blue), ESA demodulation (red), and the MFT-ESA combination (black), (e) symbol error probability comparison between 1-REC-CPM, 1-RAC-CPM and other pulse shaping functions for the proposed MFT-ESA approach.

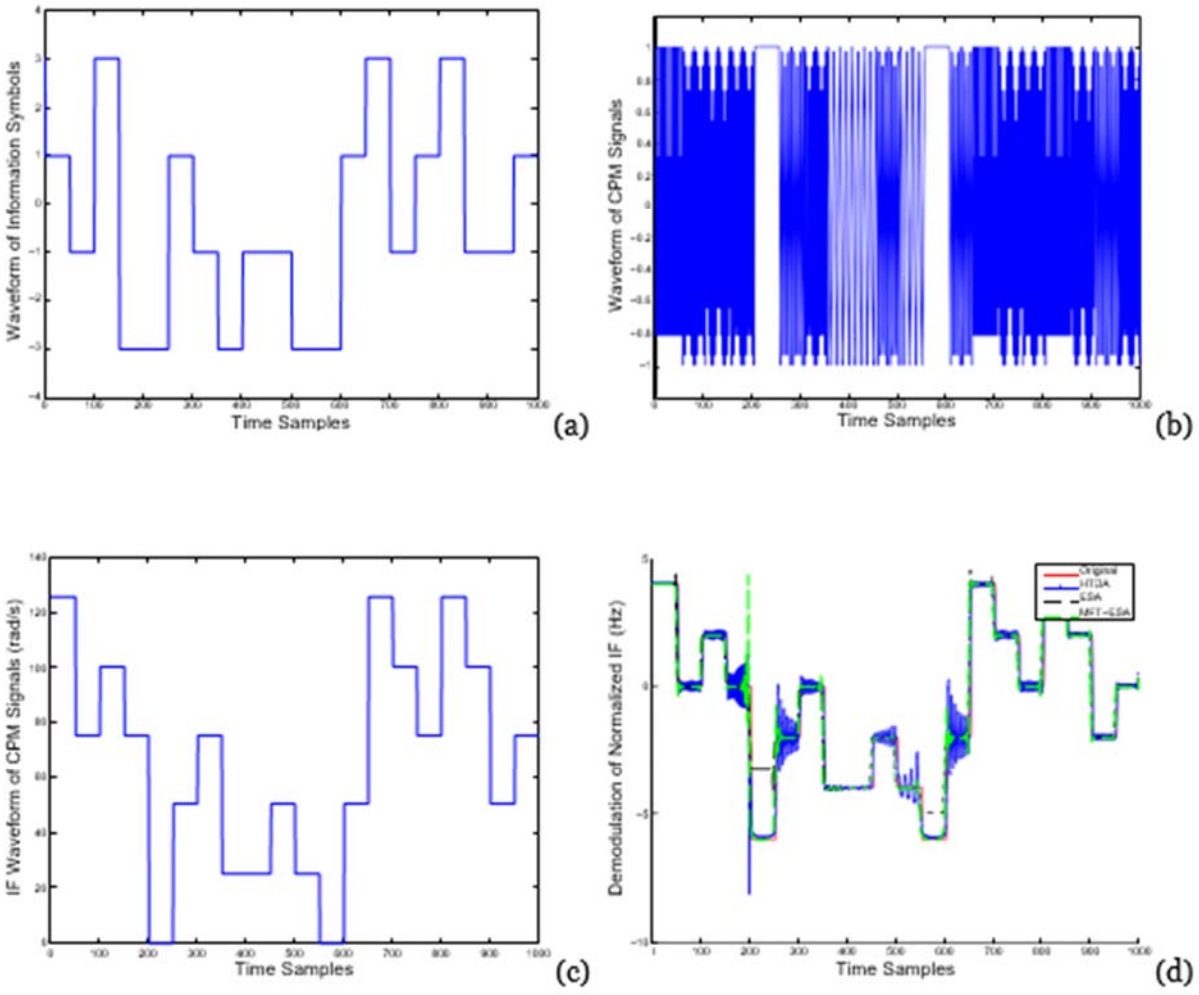

Figure 5. Multilevel 2-REC CPM with Symbols Taking Values in {−3, −1, 1, 3}

a) Modulating symbol wave- form. b) Multilevel 2-REC CPM waveform. c) IF waveform of the multilevel 2-REC CPM using rectangular pulse shaping function with memory, using $h = 4$, f_C = 12 Hz and f_S = 50 Hz and (d) demodulated IF for Hilbert transform demodulation (blue), for ESA demodulation (red), and the MFT-ESA combination (black) for R = 64.

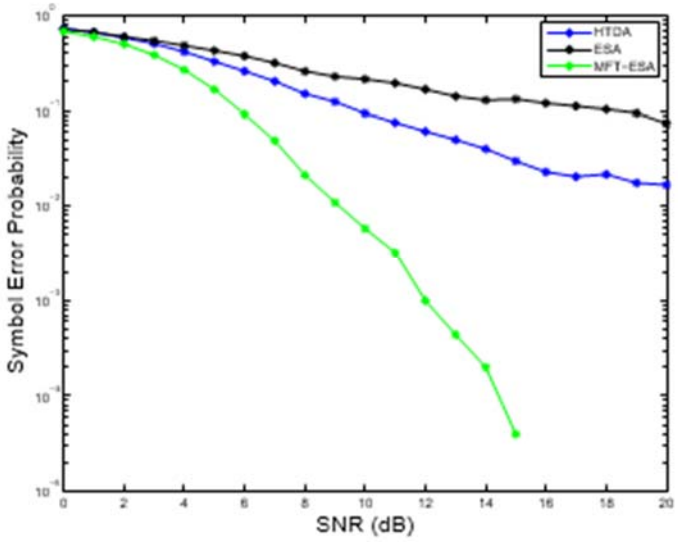

Figure 6. Multilevel 3-REC CPM Performance

Symbol error probability associated with the mixed symbols after IF estimation for 3-REC multilevel CPM.

Unlike the common AWGN channel, the noise imposed on the CPM signal is not directly added to the modulation signals (or symbols). Since the modulation signals (or symbols) are conveyed in the IF of the CPM signal, the effect of the noise remains indirect. Therefore, the symbol error performance for the CPM signal is in a different pattern than what is observed with modulation schemes that fit into the AWGN channel analysis. The CPM format provides robustness to noise when the SNR exceeds a certain threshold and if the CPM signal is sufficiently sampled.

3.2 Memory Elimination: Recursive Prediction Error Methods

The memory introduced by CPM depends on the duration of its pulse shaping function. For example, the symbol mixture incurred by L-pulsewidth CPM with Raised-cosine Pulse Shaping (L-REC CPM) is given by:

$$m(t) = \sum_{k=0}^{L-1} s(t-k) \tag{29}$$

Our goal is to recover the original symbol sequence $s(t)$ from the observation sequence $m(t)$. The observation sequence can be obtained by demodulating the CPM signals and making decisions on the demodulated IF within each symbol period. Since Equation (29) is a moving-average (MA) process, we can estimate the coefficients for Equation (29) by fitting in an Autoregressive Moving Average (ARMAX) model.

3.2.1 Background of Recursive Prediction Error Methods

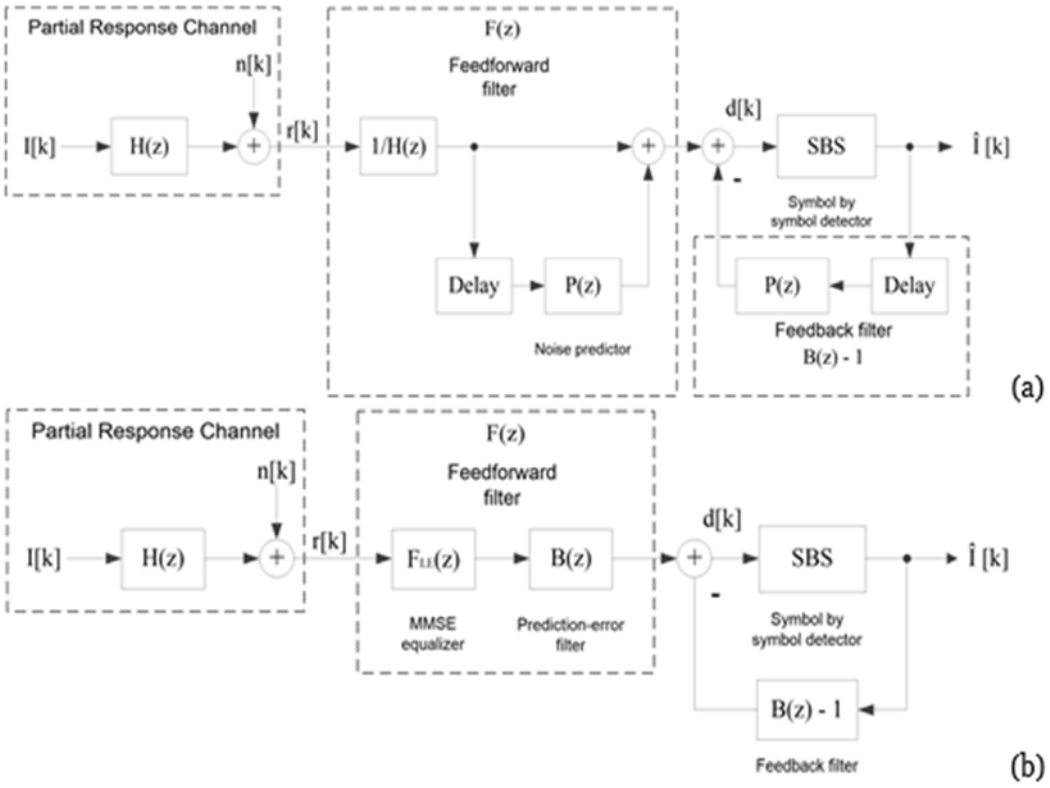

Figure 7. Block Diagrams of Both the ZF and MMSE Decision-feedback Equalizer

In our case the channel output would be the estimated IF from the MFT-ESA demodulation block.

In general, the structure of the ARMAX model is described by:

$$\sum_{k=0}^{n_a} a_k y[t-k] = \sum_{k=1}^{n_b} b_k u[t-k] + \sum_{k=0}^{n_c} c_k e[t-k] \tag{30}$$

where n_a, n_b and n_c are the number of coefficients for the Auto-regressive (AR) part, system input and MA part respectively. It can also be written as

$$A(q)y(t) = B(q)u(t) = C(q)e(t) \tag{31}$$

where q is the backward shift operator. Specifically,

$$A(q) = 1 + a_1 q^{-1} + \cdots + a_{n_a} q_1^{-n_a} \tag{32}$$
$$B(q) = b_1 q^{-1} + \cdots + b_{n_b} q^{-n_b} \tag{33}$$
$$C(q) = 1 + \ c_1 q^{-1} + \cdots + c_{n_c} q^{-n_c} \tag{34}$$

By assuming $A(q) = 1$ and $B(q) = 0$, the ARMAX model can be simplified to the MA model that exactly fits Equation (29), as described by

$$y(n) = C(q)e(t) = \sum_{k=0}^{n_c} c_k q^{-k} e(t) = \sum_{k=0}^{n_c} c_k e[t-k] \tag{35}$$

By satisfying certain conditions, $C(q)$ is actually invertible, that is, $e(n)$ can be calculated via an inverse operator $\tilde{C}(q)$ via

$$e(n) = \tilde{C}(q)y(t) = \sum_{k=0}^{\infty} \tilde{c}_k y(t-k) \tag{36}$$

The coefficient estimation for the ARMAX model can be achieved via an iterative search algorithm that minimizes a more robust quadratic prediction error criterion. The parameter vector θ can be formed by grouping the coefficients of the ARMAX model as

$$\theta = [a_1, \ldots, a_{n_a}, b_1, \ldots., b_{n_b}, c_1, \ldots., c_{n_c}] \tag{37}$$

The predictor for the ARMAX model is given by

$$C(q)\,\hat{y}(t|\theta) = B(q)u(t) + [C(q) - A(q)]y(t) \tag{38}$$

It can be rewritten as

$$\hat{y}\,(t|\theta) \quad = B(q)u(t) + [1 - A(q)]\,y(t) + [C(q) - 1]\,\varepsilon(t, \theta) \tag{39}$$

where $\varepsilon(t, \theta)$ is defined as the prediction error given by

$$\varepsilon(t, \theta) = y(t) - \hat{y}(t|\theta) \tag{40}$$

Therefore, we can express the predictor in the form of pseudolinear regression via

$$\hat{y}(t|\theta) = \varphi^T(t, \theta)\theta \tag{41}$$

where we define the data vector $\varphi(t, \theta)$ as

$$\varphi(t, \theta) = [-y(t-1), \ldots, -y(t-n\mathbf{a}), u(t-1), \ldots, u(t-n\mathbf{b}), \varepsilon(t-1, \theta), \ldots, \varepsilon(t-n\mathbf{c}, \theta)] \tag{42}$$

According to Equation (39), the gradient of the predictor $\psi(t, \theta)$ w.r.t θ can be computed via

$$C(q)\psi(t, \theta) = \varphi(t, \theta) \tag{43}$$

The gradient $\psi(t, \theta)$ can be obtained by filtering the data vector $\varphi(t, \theta)$ through an inverse filter of $C(q)$.

The cost function for the recursive prediction error method is defined as

$$V_t(\theta, \mathbf{Y}^t) = \gamma(t)\frac{1}{2}\sum_{k=1}^{t}\beta(t,k)\epsilon^2(k,\theta) \tag{44}$$

where $\beta(t, k)$ and $\gamma(t)$ satisfy the following conditions

$$\beta(t,k) = \prod_{j=k+1}^{t}\lambda(j), \qquad \beta(t,t) = 1, \tag{45}$$

$$\sum_{k=1}^{t}\gamma(t)\beta(t,k) = 1 \tag{46}$$

Note that $\lambda(j)$ is the forgetting factor, which is often set to a constant less than 1. The algorithm of the recursive prediction error method is then summarized via

$$\varepsilon(t) = y(t) - \hat{y}(t), \tag{47}$$

$$\hat{\theta}(t) = \hat{\theta}(t-1) + \gamma(t)\, R^{-1}(t)\, \psi(t)\, \varepsilon(t), \tag{48}$$

$$R(t) = R(t-1) + \gamma(t)\, [\psi(t)\, \psi\ (t)^{\mathrm{T}} - R(t-1)] \tag{49}$$

where $\psi(t)$ and $\hat{y}(t)$ are short for the resulting approximations of $\psi(t, \hat{\theta}(t-1))$ and $\hat{y}(t|\theta(t-1))$ respectively.

The experimental results for a 3-REC multilevel CPM case is illustrated by Figure 8(a). With a memory length $L = 3$, Equation (29) for the 3-REC multilevel CPM can be written as

$$m[t] = s[t] + c1\ s[t-1] + c2\ s[t-2], \tag{50}$$

where $c1 = c2 = 1$. As we can observe, the estimated coefficients finally converge close to the true value of 1 in the case of REC-CPM. They serve as useful estimates when other forms of pulse shaping such as in RAC-COM or SRAC-CPM are employed.

3.2.2 Symbol Recovery Via Equalization

3.2.2.1 ZF-DFE Solution

By inverting the MA process using the estimated coefficients of the MA model, the original symbol sequence can be recovered by applying the inverse filter $Hinv\,(q)$ on the observation sequence $m(t)$ and classifying the filter output according to the optimal region of each symbol. For the previous case of the 3-REC multilevel CPM, the expression for the inverse filter is given by

$$H_{inv}(q) = \frac{1}{1 + \widehat{c_1} q^{-1} + \widehat{c_2} q^{-2}} \tag{51}$$

Note that the inverse filter $Hinv\,(q)$ is an IIR All-pole filter, which can be implemented via direct recursion of its difference equation. It requires the input, i.e., in our case, the mixed symbols, to be nearly perfect, otherwise the error incurred by inaccurate input symbols can be significant. This in turn requires the MFT-ESA demodulation section to produce a sufficiently accurate demodulation result. By incorporating the slicer, i.e., the symbol by symbol detection device into the inverse filter recursion we can implement the decision feedback version of the zero-forcing equalizer (ZF-DFE) to eliminate memory induced by partial response signaling in the 3-REC CPM signal.

3.2.2.2 MMSE-DFE Solution

Instead of focusing on just removal of the channel between the IF input and the input symbols if we further incorporate a MMSE cost function that balances the task of eliminating memory with the task of reducing symbol distortion, then we obtain the linear MMSE equalizer that can provide further improvement in the symbol error performance at the expense of training using pilot symbols for channel estimation. The corresponding decision feedback version of the linear MMSE equalizer (MMSE-DFE) incorporates both pre-cursor and post-cursor taps as described in [1]. The feedforward filter coefficients of the MMSE-DFE are obtained from the Wiener solution and then used to solve for the feedback filter coefficients.

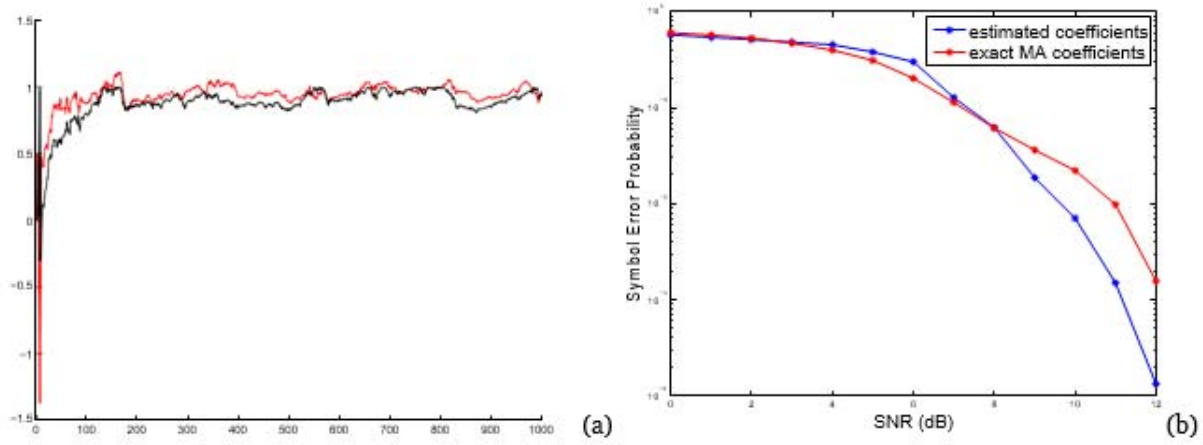

Figure 8. Multilevel CPM with Memory

(a) MA model coefficient estimation for 3-REC multilevel CPM with symbols taking values in $\{-3, -1, 1, 3\}$. Note that the red line indicates the convergence of the estimated coefficient $\hat{c}_1$ and the black line indicates the convergence of the estimated coefficient $\hat{c}_2$ and (b) final symbol error probability for 3-REC multilevel CPM using the recursive prediction error method for memory elimination using the zero-forcing (ZF-DFE), i.e., the estimated coefficient values and rounded output and the actual values of the MA model coefficients.

4.0 Results and Discussion

The MFT-ESA demodulation module described in the prior sections is then combined with recursive prediction approach for memory removal to obtain estimates of the original information symbols. The symbol error probability for a 3-REC multilevel CPM case is illustrated by Figure 8(b) for both the zero-forcing solution, i.e., inverse filtering using the coefficient estimates from the recursive predictive approach, and the zero-forcing decision feedback solution that uses the rounded output of inverse filtering from one instant towards the next instant. From our previous analysis, we know that the error associated with the mixed symbols extracted from the demodulated IF for low SNR is significant. The recovery of the original symbols for low SNR, is significantly influenced since the proposed memory elimination approach is very sensitive to its input of mixed symbols. However, as the SNR increases, the input of the mixed symbols becomes more accurate, thereby resulting in significant improvement in the ability to recover the original symbols as evidenced in the symbol probability. Above a SNR threshold of around 12 dB, the symbol error probability becomes zero, attributable to the fact that inverse filtering solution becomes perfect after that threshold.

A further limitation of the Viterbi algorithm is that it requires complete information regarding the setup of CPM signals, for example, the modulation index h, symbol alphabet size M and memory length L, to determine the state trellis, while the proposed algorithm has the potential to predict the setup of CPM signals if some amount of training is allowed. A 4-REC multilevel case is illustrated by Figure 10 to prove that the proposed method can estimate the pulse length L of the CPM signals.

By fitting the ARMAX model with different memory lengths, we can compare the symbol error performance of each setting to determine the correct memory length. From Figure 10, we can see that if the fitted length is smaller than the correct length, the symbol error is significant. By fitting the model with the correct length $L = 4$, the symbol error drops dramatically. Once the fitted length is larger than the correct memory length, the error either remains at a low level or will increase dramatically. Such a pattern reveals the potential of the proposed method in determining the correct pulse length of the CPM environment.

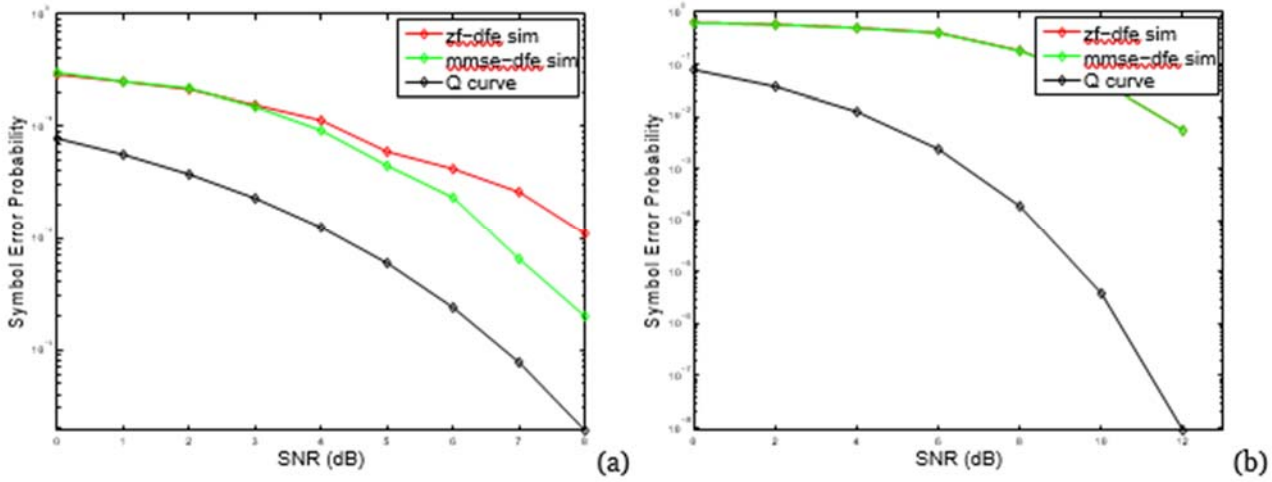

Figure 9. Memory Removal via Equalization

(a) symbol error probability of MFT-ESA approach for binary CPFSK with zero-forcing and MMSE decision feedback equalization to remove memory induced due to partial response signaling, and (b) symbol error probability for multilevel CPFSK with zero-forcing and MMSE decision feedback equalization. In both cases 3-REC-CPM with parameters $T_b = 1s$, $f_b = 50Hz$, $f_c = 12Hz$ was employed. The MFT conversion factor was $R = 16$ and the modulation indices for the binary and multilevel cases were $h = 97/21$ and $h = 19/15$ respectively. For equalization purposes, 50 pilot symbols were used corresponding to 25-percent training.

5.0 CONCLUSIONS

In this report, we have presented an approach towards wideband CPM demodulation by extending the MFT-ESA approach developed by the authors. The characteristic features of the proposed MFT-ESA approach are:

1. Unlike the Viterbi algorithm that requires that restricts the modulation index via gcd(*m, p*) = 1, there are no restrictions on the modulation index in the proposed approach.

2. Unlike the Viterbi algorithm whose complexity increases with *m* and *p*, the complexity of the proposed approach is independent of the modulation index.

3. The proposed approach does not require prior knowledge of the carrier frequency and this parameter can be extracted from the IF estimates.

4. The proposed approach can handle large modulation indices and multilevel signaling making it conducive to the large bandwidth requirements proposed in the Mary FSK system for satellite communications [6].

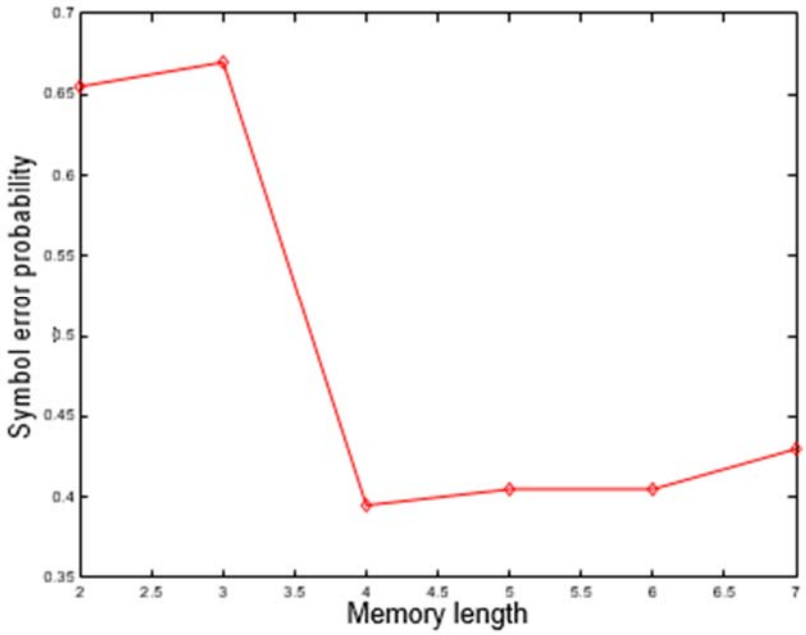

Figure 10. Symbol Error Performances

For 4-REC multilevel CPM by fitting the ARMAX model with different pulse length *L*.

The proposed MFT-ESA approach was then applied to the demodulation of CPM signals with partial response signaling, where memory is introduced into the estimated IF. Post the MFT-ESA demodulation stage, a recursive prediction approach, based on MA signal modeling of the estimated IF, was presented to address the problem of removal of memory introduced due to partial response signaling via equalization. Both the zero-forcing solution based on direct inversion of the memory channel, its corresponding decision feedback version and the MMSE-DFE solution to memory removal were investigated and shown to produce significant reduction in the symbol error probability over no equalization. The recursive prediction approach also provides a means to estimate the correct memory length that is required for the Viterbi algorithm.

REFERENCES

[1] J. G. Proakis and Masoud Salehi, "Digital Communications," Fifth edition, McGraw-Hill Publishing Company, New York, 1995.

[2] A. Potamianos and P. Maragos, "A Comparison of the Energy Operator and Hilbert Transform Approach to Signal and Speech Demodulation," *Signal Processing*, Vol. 37, No. 1, pp. 95-120, 1994.

[3] E. Bedrosian, "Trans-ionospheric propagation of FM signals," RM-5369- NASA, RAND Memorandum, August 1967.

[4] A.J. Giger and J. G. Chafee, "The FM Demodulator with Negative Feedback," The Bell System Technical Journal, Vol. 42, Issue 4, pp. 1109-1135, Jul 1963.

[5] M. Fitch and K. Briggs, "Gaussian Multilevel FM for High-bandwidth Satellite Communications," University College of London, 2004, http://www.ee.ucl.ac.uk/~fstentif/MGFSK_paper.pdf.

[6] S. Bellini and G. Tartara, "Efficient Discriminator Detection of Partial Response Continuous Phase Modulation," *IEEE Transactions on Communications*, Vol. 33, No. 8, pp. 883-886, Aug. 1985.

[7] P. Maragos, J. F. Kaiser, and T. F. Quatieri, "Energy separation in signal modulations with application to speech analysis," *IEEE Transactions on Signal Processing*, Vol. 41, No. 10, pp. 3024 - 3051, Oct 1993.

[8] Balu Santhanam, "Generalized Energy Demodulation for Large Frequency Deviations and Wideband Signals," *IEEE Signal Processing Letters*, Vol. 11, No. 3, pp. 341-344, 2004.

[9] Malay Gupta and Balu Santhanam, "Adaptive linear predictive frequency tracking and CPM demodulation," *Proc. Asilomar Conference on Signals, Systems, and Computers*, Pacific Grove, CA, Vol. 1, pp. 206, 2004.

[10] Wenjing Liu and Balu Santhanam, "Wideband-FM Demodulation For Large Wideband To Narrowband Conversion Factors Via Multirate Frequency Transformation," *Proc. of Signal Processing and SP Education Workshop*, Salt Lake City, UT, pp. 97-102, 2015.

[11] Michael J. Gertsman and John H. Lodge, "Symbol-by-Symbol MAP Demodulation of CPM and PSK Signals on Rayleigh Flat-Fading Channels," *IEEE Transactions on Communications*, Vol. 45, No. 7, pp. 788 - 799, July 1997.

[12] S. S. Abayesekara, "Robust full response Mary raised-cosine CPM receiver design via frequency estimation," *Proc. of International Conference on DSP*, Singapore, pp. 935-939, 2015.

[13] J. B. Anderson, T. Aulin and C-E. W. Sundberg, Digital Phase Modulation, Springer, New York, 1986.

[14] C-E. W. Sundberg, "Continuous Phase Modulations Part I and II," *IEEE Communications Magazine*, Vol. 24, pp. 25-38, April 1986.

LIST OF SYMBOLS, ABBREVIATIONS AND ACRONYMS

2-REC CPM	Binary CPM with rectangular pulse shaping
AM–FM	Amplitude modulation frequency modulation
AR	Auto-regressive
ARMAX	Autoregressive-moving average
AWGN	Additive white Gaussian noise
BPSK	Binary phase shift keying
CESA	Continuous energy separation algorithm
CPM	Continuous phase modulation
CR/FD	Carrier to frequency deviation ratio
CR/IB	Carrier to Information Bandwidth Ratio
DAC	Digital to analog convertor
DFE	Decision feedback equalizer
ESA	Energy separation algorithm
FIR	Finite impulse response
FM	Frequency Modulation
FSK	Frequency Shift Keying
GMSK	Gaussian minimum shift keying
GSM	Global System for Mobile communications
HTDA	Hilbert transform alone
IA	Instantaneous amplitude
IF	Instantaneous frequency
L-RAC CPM	L-pulsewidth CPM with rectangular pulse shaping
L-REC CPM	L-pulsewidth CPM with raised-cosine pulse shaping
MA	Moving-average
MFT-ESA	Multirate Frequency Transformation-Electronics Steered Array
MFT	Multirate frequency transformation
ML	Maximum Likelihood
MMSE-DFE	MMSE Decision Feedback Equalizer
NMSE	Normalized mean square error
PAM	Phase amplitude modulation
SNR	Signal-to-noise Ratio
ZF-DFE	Zero Forcing Decision Feedback Equalizer

DISTRIBUTION LIST

DTIC/OCP
8725 John J. Kingman Rd, Suite 0944
Ft Belvoir, VA 22060-6218 1 cy

AFRL/RVIL
Kirtland AFB, NM 87117-5776 1 cy

Official Record Copy
AFRL/RVSW/Khanh Pham 1 cy